Biosensors and Bioelectronics 227 (2023) 115146

Contents lists available at ScienceDirect

Biosensors and Bioelectronics

journal homepage: www.elsevier.com/locate/bios

Smartphone-based 3D-printed electrochemiluminescence enzyme biosensor for reagentless glucose quantification in real matrices

Donato Calabria [a,b], Elisa Lazzarini [a], Andrea Pace [a], Ilaria Trozzi [a], Martina Zangheri [a,c,d], Stefano Cinti [e,f], Marinella Difonzo [a], Giovanni Valenti [a], Massimo Guardigli [a,b,g], Francesco Paolucci [a,*], Mara Mirasoli [a,b,g,**]

[a] Department of Chemistry "Giacomo Ciamician", Alma Mater Studiorum - University of Bologna, Via Selmi 2, I-40126, Bologna, Italy
[b] Interdepartmental Centre for Industrial Aerospace Research (CIRI AEROSPACE), Alma Mater Studiorum-University of Bologna, Via Baldassarre Canaccini 12, I-47121, Forlì, Italy
[c] Interdepartmental Centre for Industrial Agrofood Research (CIRI AGRO), Alma Mater Studiorum - University of Bologna, Via Quinto Bucci 336, I-47521, Cesena, Italy
[d] Interdepartmental Centre for Industrial Research in Advanced Mechanical Engineering Applications and Materials Technology (CIRI MAM), Alma Mater Studiorum-University of Bologna, Viale Risorgimento 2, I-40136, Bologna, Italy
[e] Department of Pharmacy, University Naples Federico II, Via Domenico Montesano 49, I-80131, Naples, Italy
[f] BAT Center–Interuniversity Center for Studies on Bioinspired Agro-Environmental Technology, University of Napoli "Federico II", 80055, Portici, Naples, Italy
[g] Interdepartmental Centre for Industrial Research in Renewable Resources, Environment, Sea and Energy (CIRI FRAME), Alma Mater Studiorum - University of Bologna, Via Sant'Alberto 163, I-48123, Ravenna, Italy

ARTICLE INFO

Keywords:
3D printing
Biosensor
Conductive PLA
Electrochemiluminescence
Glucose
Luminol

ABSTRACT

Three-dimensional (3D) printed electrochemical devices are increasingly used in point-of-need and point-of-care testing. They show several advantages such as simple fabrication, low cost, fast response, and excellent selectivity and sensitivity in small sample volumes. However, there are only a few examples of analytical devices combining 3D-printed electrodes with electrochemiluminescence (ECL) detection, an electrochemical detection principle widely employed in clinical chemistry analysis. Herein, a portable, 3D-printed miniaturized ECL biosensor for glucose detection has been developed, based on the luminol/H_2O_2 ECL system and employing a two-electrode configuration with carbon black-doped polylactic acid (PLA) electrodes. The ECL emission is obtained by means of a 1.5V AA alkaline battery and detected using a smartphone camera, thus providing easy portability of the analytical platform. The ECL system was successfully applied for sensing H_2O_2 and, upon coupling the luminol/H_2O_2 system with the enzyme glucose oxidase, for glucose detection. The incorporation of luminol and glucose oxidase in an agarose hydrogel matrix allowed to produce ECL devices preloaded with the reagents required for the assay, so that the analysis only required sample addition. The ECL biosensor showed an excellent ability to detect glucose up to 5 mmol L^{-1}, with a limit of detection of 60 μmol L^{-1}. The biosensor was also used to analyse real samples (i.e., glucose saline solutions and artificial serum samples) with satisfactory results, thus suggesting its suitability for point-of-care analysis. Coupling with other oxidases could further extend the applicability of this analytical platform.

1. Introduction

Three-dimensional (3D) printing, which relies on the layer-by-layer addition of materials (additive manufacturing), is gaining increasing interest in the biosensors field, as it enables easy, rapid, reproducible, and low-cost prototyping and production of device components, even of complex geometries. The fast and almost direct design-to-object workflow provides great flexibility in the design and optimization of the analytical system (Ali et al., 2022; Palenzuela and Pumera, 2018). In addition, 3D printing is considered an environment-friendly process as it generates minimal waste and enables in-house production, thus reducing the environmental impacts of transportation and storage.

3D printing has been used for manufacturing a variety of biosensor components, such as microfluidic chips (Arshavsky-Graham et al., 2021;

* Corresponding author. Department of Chemistry "Giacomo Ciamician" Alma Mater Studiorum - University of Bologna, via Selmi 2, Bologna, Italy.
** Corresponding author. Department of Chemistry "Giacomo Ciamician" Alma Mater Studiorum - University of Bologna, via Selmi 2, Bologna, Italy.
E-mail addresses: francesco.paolucci@unibo.it (F. Paolucci), mara.mirasoli@unibo.it (M. Mirasoli).

https://doi.org/10.1016/j.bios.2023.115146
Received 20 November 2022; Received in revised form 21 January 2023; Accepted 8 February 2023
Available online 10 February 2023

Calabria et al., 2020; Chiado et al., 2020; Kadimisetty et al., 2017), analytical cartridges (Van Nguyen et al., 2019; Zangheri et al., 2019), optical components (Lertvachirapaiboon et al., 2021; Roda et al., 2019), smartphone interfaces (Calabria et al., 2021b; Lai et al., 2022; Li et al., 2017), analytical device components (Calabria et al., 2021a; Liu et al., 2020; Mustafa et al., 2021), and wearable devices (Kalkal et al., 2021). More recently, energy storage devices and electrodes for electroanalytical applications have been also produced (Cardoso et al., 2020; Marzo et al., 2020; Omar et al., 2021; Silva et al., 2022) employing commercially available or in-house fabricated conductive thermoplastic materials, obtained by incorporating into polymers conductive nanomaterials such as carbon nanotubes, carbon black, and graphene. This approach has helped to overcome some limitations due to the manual fabrication of electrochemical biosensors (e.g., poor reproducibility), as well as to improve the overall analytical performance (Cardoso et al., 2020; Omar et al., 2021).

Electrochemiluminescence (ECL), a luminescent phenomenon induced by an electrochemical stimulus on a specific molecular system (Richter, 2004; Miao, 2008), is one of the leading transduction techniques in biosensing (Fiorani et al., 2019; Qi and Zhang, 2020; Yoo et al., 2022). As compared with photoluminescence and chemiluminescence, it provides superior temporal and spatial control of light emission, very low background, high sensitivity, broad dynamic range, and rapid measurement (Du et al., 2021; Hesari and Ding, 2015; Liu et al., 2015; Lv et al., 2020; Nasrollahpour et al., 2022; Sojic, 2020). In addition, with respect to other electrochemical techniques ECL is less sensitive to electrical interferences and can exploit simplified electric circuit devices, since photon emission is measured instead of current (Ma et al., 2021). Owing to these characteristics, ECL is particularly appealing for the development of portable biosensing devices (Doeven et al., 2015; Gao et al., 2018; Nikolaou et al., 2022; Pittet et al., 2008; Yoo et al., 2022). In the last two decades, integration of biosensors into smartphone-based systems has been demonstrated a unique opportunity for widespread availability of portable devices (Huang et al., 2018; Quesada-Gonzalez and Merkoci, 2017). Delaney et al. first proposed a smartphone-based microfluidic biosensor exploiting the mobile phone camera for ECL measurement (Delaney et al., 2011), paving the way for an ever-increasing number of publications in this field (Doeven et al., 2015; Li et al., 2019; Yao et al., 2017; Zhang et al., 2022).

Despite of its potential advantages, 3D printing has been poorly exploited in ECL (Bishop et al., 2016; Climent and Rurack, 2021; Kadimisetty et al., 2017; Motaghi et al., 2018; Zhan et al., 2022) and only a few biosensing devices exploiting 3D-printed electrodes have been proposed so far (Bhaiyya et al., 2022a, 2022b; Douman et al., 2021). Herein we combined 3D printing technology with ECL transduction for developing a smartphone-based biosensor for glucose detection in biological samples. The biosensor relied on the glucose oxidation catalysed by glucose oxidase (GO), followed by the ECL detection of the produced hydrogen peroxide. Luminol was employed as the ECL reagent, taking advantage of its low oxidation potential and high emission yield (Aymard et al., 2017; Leca-Bouvier et al., 2020; Ma et al., 2021; Rahmawati et al., 2022). With respect to previously published work (Bhaiyya et al., 2022a, 2022b), our biosensor displays improved features for point-of-care application, such as a simple electrical circuit and a ready-to-use format, in which all the reagents are prestored into the device.

2. Materials and methods

2.1. Reagents and materials

Glucose oxidase (GO, from *Aspergillus niger*, ≥250 U mg^{-1} solid), luminol (5-amino-2,3-dihydro-1,4-phthalazindione sodium salt), hydrogen peroxide (30% (v/v) aqueous solution), β-D-glucose, and agarose were purchased from Merck KGaA (Darmstadt, Germany). All the other chemicals employed were of the highest purity available. Artificial serum was prepared following a published composition (Basiaga et al., 2014) to which 35 g L^{-1} Human Serum Albumin was added.

The enzymatic colorimetric assay (Glucose Colorimetric Detection Kit) in the 96-well microplate format used as a reference method for assessing glucose concentration of real samples was bought from Life Technologies Corporation Thermo Fisher Scientific (Frederick, MD).

The conductive Protopasta composite PLA (PLA loaded with about 20% of carbon black, resistivity 15 Ω cm) and the conventional PLA polymers were from Protoplant Inc. (Vancouver, WA) and MakerBot Industries (New York, NY), respectively.

2.2. Data analysis and processing

Quantitative analysis of ECL images was performed using the freeware ImageJ v.1.53s software (National Institutes of Health, Bethesda, MD). GraphPad Prism v.8.3.0 software (GraphPad Software, San Diego, CA) was employed for data graphing and regression analysis.

2.3. Electroanalytical device

The ECL device components (Fig. 1a and b) were designed using SketchUp Pro v.2021 CAD software (Trimble Inc., Sunnyvale, CA) and manufactured from PLA polymer, either conductive (for working and auxiliary electrodes) or non-conductive (for spacer), using a commercial Fused Deposition Modelling (FDM) 3D printer (MakerBot Replicator 2X, MakerBot Industries). The components were then assembled using a cyanoacrylate-based glue and a plastic layer with transparent pressure-sensitive adhesive was applied to the bottom of the ECL device to create the measurement cell (about 100 μL of volume).

2.4. Cyclic voltammetry measurements

Cyclic voltammetry (CV)/ECL and electrochemical measurements were conducted with a SP-300 potentiostat (Biologic, Seyssinet-Pariset, France) using the electroanalytical device described below together with an Ag/AgCl external reference electrode. The ECL signal was measured with a R928 photomultiplier tube (Hamamatsu Photonics K.K., Shizuoka, Japan) supplied with 750 V and placed at a fixed height from the electrochemical cell, inside a dark box. A high-voltage power supply socket assembly with a transimpedance amplifier (C6271, Hamamatsu Photonics K.K.) was employed to the photomultiplier, using an external trigger connection to the potentiostat DAC module. Light/current/potential curves were recorded by collecting the amplified photomultiplier output signal with the ADC module of the potentiostat.

2.5. Analytical system for the solution based ECL device

The ECL emission was acquired with an ATIK 11000 Charge-Coupled Device (CCD) camera (ATIK Cameras, New Road, Norwich) equipped with a dark box to avoid interference from ambient light during the measurement. The camera employed a large format, high resolution Kodak KAI 11002 monochrome sensor cooled down to 5 °C by a two-stage Peltier element to reduce thermal noise. The CCD sensor was coupled with a 25 × 25 mm^2 fibre optic faceplate in a contact imaging configuration as previously described (Roda et al., 2011). For ECL measurements, the ECL device was positioned inside the dark box in correspondence with the fibre optic faceplate and a 1.5 V voltage was applied to the electrodes using a variable voltage DC power supply.

2.6. Assay procedures for the solution-based ECL device

For the quantification of hydrogen peroxide, 40 μL of H_2O_2 standard solution or water (for blank) were dispensed in the measurement cell of the ECL device. Then, 40 μL of a 10 mmol L^{-1} luminol solution in 0.2 mol L^{-1} carbonate buffer (pH 10.8) was added prior to application of the

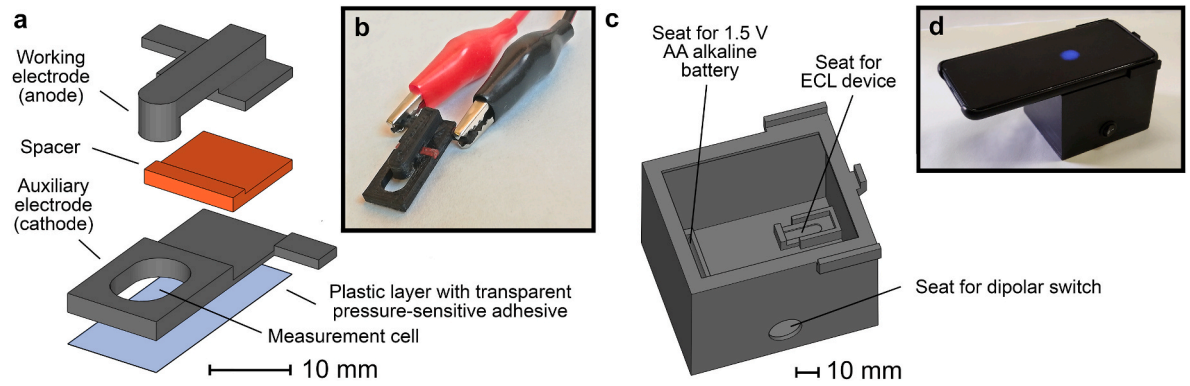

Fig. 1. (a) Scheme and (b) photograph of the 3D-printed ECL device. Black and orange components were produced in conductive and non-conductive PLA polymer, respectively. (c) Scheme of the 3D-printed dark box used to perform ECL measurements with the hydrogel-based ECL device employing a smartphone for the detection of the ECL emission and (d) photograph of the analytical system during a measurement.

voltage. The ECL emission was measured over a period of 100 s acquiring a series of 20 consecutive images (exposure time 5 s). The voltage was applied to the ECL device 20 s after the starting of the acquisition, thus the first four images could be used for evaluation of the background signal. For the quantification of glucose, 40 μL of glucose standard solution, water (for blank) or sample (if necessary, appropriately diluted with water to obtain a glucose concentration within the assay calibration range) were dispensed in the measurement cell, followed by 10 μL of a 1.25 U μL^{-1} GO solution in 0.1 mol L^{-1} phosphate buffer (pH 7.0). After a 15 min-incubation period, 40 μL of a 10 mmol L^{-1} luminol solution in 0.2 mol L^{-1} carbonate buffer (pH 10.8) was added and the ECL emission was measured as described before.

For each experiment the acquired images were analysed to evaluate the signal, i.e., the sum of the pixel intensities over the region of interest (ROI) area corresponding to the anode of the ECL device. The background (e.g., due to thermal and readout noise of the CCD camera as well as to CL emission from the spontaneous oxidation of luminol) was calculated as the mean of the signals obtained for the first four images of the sequence, then the kinetic profile of the ECL emission was generated by plotting the background-subtracted ECL emission intensity vs. time. Finally, the ECL signal of each experiment was calculated by integrating the ECL emission kinetic profile over the 20–80 s time interval. The assay calibration curves were generated by graphing the blank-subtracted ECL signals obtained for H_2O_2 (or glucose) standard solutions vs. the logarithm of analyte concentration and fitting the experimental data by a first-order polynomial equation, and the concentrations of unknown H_2O_2 (or glucose) samples were calculated by interpolation of their blank-subtracted ECL signals on the calibration curve.

2.7. Hydrogel-based ECL biosensor

The hydrogel-based ECL biosensor for the measurement of H_2O_2 was produced by dispensing in the measurement cell 100 μL of a hot 0.1 mol L^{-1} carbonate buffer solution (pH 10.8) containing 0.8% (m/v) agarose and 5 mmol L^{-1} luminol. After cooling to room temperature, a luminol-functionalized agarose hydrogel was obtained. The ECL device for the measurement of glucose was obtained in a similar way, except that the solution dispensed into the device also contained 0.125 U μL^{-1} of GO (the enzyme was added just before dispensation of the solution into the device to avoid thermal degradation).

2.8. Analytical system for the hydrogel-based ECL biosensor

Detection of the ECL emission was performed with a Samsung S20 smartphone (Samsung, Seoul, South Korea) using the proprietary camera app. A 3D-printed dark box produced in black PLA (Fig. 1c and d) prevented interference from ambient light during the ECL measurement and ensured the correct positioning of the ECL device with respect to the smartphone camera (the device was positioned with the auxiliary electrode at the top, so that the ECL emission at the working electrode would be visible by the camera). A 1.5V AA alkaline battery and a bipolar switch allowed generation and control of the ECL emission.

2.9. Assay procedures for the hydrogel -based ECL biosensor

The plastic adhesive layer was removed to expose the bottom surface of the hydrogel, then the device was inserted in the black box with the auxiliary electrode at the top. For the quantification of hydrogen peroxide in the luminol-functionalized ECL biosensor, 40 μL of H_2O_2 standard solution or water (for blank) were dispensed on the hydrogel. After 15 min the solution was absorbed into the hydrogel and two image acquisitions (60 s exposure time, ISO 3200 sensitivity) were performed with the smartphone. The first image was acquired without applied voltage, while the second one was acquired with the 1.5 V voltage applied to the ECL device. For the quantification of glucose in the luminol/GO-functionalized ECL biosensor, 40 μL of glucose standard solution, water (for blank) or sample (if necessary, diluted with water) were dispensed on the hydrogel, then the measure was performed as described before.

For each experiment the acquired images were analysed to evaluate the signal (the first image provided for the value of the background, which was subtracted from the signal calculated for the second image to obtain the actual ECL signal of the experiment). Then, the H_2O_2 (or glucose) calibration curves were generated by graphing the logarithm of the blank-subtracted ECL signal vs. the logarithm of analyte concentration and fitting the experimental data by a first-order polynomial equation. The concentrations of unknown H_2O_2 (or glucose) samples were calculated by interpolation of their blank-subtracted ECL signals on the calibration curve.

3. Results and discussion

3.1. Solution-based ECL device

The ECL device employed a simple two-electrode configuration without any reference electrode (Gao et al., 2020; Pan et al., 2014; Wang et al., 2012). Although in such configuration the potential of the working electrode cannot be controlled, this approach simplified both the ECL device and the analytical system (ECL measurements could be performed using a low-cost variable voltage power supply or even a 1.5V alkaline battery). The 3D printing technology allowed to produce a device with a complex shape (which included a measurement cell in which reagents and sample could be directly dispensed), using PLA, a

(bio)polyester that is considered an environment-friendly material.

3.1.1. Optimization of experimental conditions

To characterize the ECL device we firstly studied the ECL emission as a function of the applied potential (with respect to an Ag/AgCl external reference electrode) in CV experiments. In agreement with literature data (Leca-Bouvier et al., 2020; Pittet et al., 2007; Zhou et al., 2022) the ECL emission vs. potential profile (Fig. 2a) presented a peak starting at about 0.7–0.75 V vs. Ag/AgCl due to the oxidation of both luminol and H_2O_2. A summary of the reactions leading to the ECL signal generation, as hypothesized by Zhou et al. (2022), is reported in Scheme 1. Taking into consideration such result, the ECL measurements in the device were performed by applying a 1.5 V voltage between the electrodes.

Imaging measurements were also performed during CV/ECL experiments to assess the spatial localization of the ECL emission, which, as expected, was produced at the anode of the ECL device (Fig. 2b and c).

The ECL signal of the luminol/H_2O_2 system is strongly influenced by the luminol concentration and the pH of the working medium. Fig. 3a reports the ECL emissions obtained in 0.1 mmol L^{-1} H_2O_2 solutions containing different concentrations of luminol. An increase of the ECL emission intensity with the concentration of luminol has been observed up to 5.0 mmol L^{-1}, while more concentrated luminol solutions gave weaker ECL signals, which can be ascribed to a self-quenching effect (Zhang et al., 2016). Based on these results, a 5.0 mmol L^{-1} luminol concentration was selected to be used in the ECL device.

Once established the optimal luminol concentration, the effect of pH on the ECL emission was investigated. It is indeed known that the luminol/H_2O_2 ECL system is more efficient at alkaline pH because the oxidized, unprotonated form of luminol (diazaquinone) reacts with the HO_2^- anion (Leca-Bouvier et al., 2020). To this end, ECL measurements were performed in 0.1 mol L^{-1} buffer solutions with pH values ranging from 7.4 to 10.8 and in NaOH solution at pH 13.0. Each solution was tested either without or with different concentrations of H_2O_2 to evaluate the dynamic range of the H_2O_2 ECL assay. As shown in Fig. 3b, at lower pH values (pH 7.4 and 8.5) weak ECL signals were obtained and the signal due to oxidation of hydrogen peroxide could not be discriminated from the blank, except at the highest concentration. The measurements performed at pH 10.8 provided much more intense ECL signals as well as an evident increasing trend with the concentration of hydrogen peroxide. The ECL signals were even higher at pH 13.0, however the dynamic range was reduced because of the intense blank signal. Therefore, the carbonate buffer was selected as that providing the widest dynamic range of the hydrogen peroxide assay. This finding is in line with the literature since pH values around 10 were found to provide the highest signal-to-background ratios for the luminol/H_2O_2 CL (Calabria et al., 2021b) and ECL systems (Zhou et al., 2022).

3.1.2. Quantification of hydrogen peroxide

As a preliminary step for the development of the glucose ECL biosensor, the performance of the ECL device in the quantification of H_2O_2 was evaluated. Fig. 4a and b show, respectively, the kinetic profiles of the ECL emissions obtained by analysing H_2O_2 standard solutions and the corresponding H_2O_2 calibration curve (the evaluation of the ECL signal as the integral of the ECL emission over a 60 s-time interval starting from the application of the voltage to the ECL device was preferred to the measurement of the peak ECL intensity since it reduced data variability). A good correlation between the ECL analytical signal and the logarithm of the H_2O_2 concentration was found in the 0.05–5.0 mmol L^{-1} concentration interval, and the detection limit (LOD) of the assay (estimated as the concentration of H_2O_2 giving a signal corresponding to that of the blank plus three times its standard deviation) was about 40 μmol L^{-1}.

3.1.3. Quantification of glucose

The ECL biosensor for glucose was designed to exploit an endpoint assay, i.e., the glucose was completely oxidized to gluconic acid and hydrogen peroxide in the GO-catalysed enzyme reaction before performing the ECL measurement of H_2O_2. This increased assay sensitivity (the amount of H_2O_2 to be detected is the highest possible) but required a preliminary incubation step (15 min in our case) for glucose oxidation. In addition, the optimal pH for the GO-catalysed enzyme reaction is slightly acidic, even though a quite broad pH range of activity (pH 4–7) has been reported (Tsuge et al., 1975). Therefore, the incubation step was carried out at pH 7.0, then the pH value was adjusted to 10.8 by adding a concentrated carbonate buffer solution prior to ECL measurement (Kitte et al., 2017).

Fig. 4c shows the kinetic profiles of the ECL emissions obtained by analysing glucose standard solutions. The behaviour of the kinetic profiles was like that found for the H_2O_2 assay, even though the decrease of the ECL emission with time was slightly faster. The corresponding glucose calibration curve (Fig. 4d) covered the 0.05–2.0 mmol L^{-1} concentration interval, with a CV% below 10%. The LOD of the assay (about 50 μmol L^{-1} of glucose) was of the same order of magnitude of that found for H_2O_2. The performance of the ECL glucose biosensor was also tested in real samples. Glucose saline solutions with glucose contents ranging from 5% to 70% (m/v) were diluted 1:2000 (v/v) with water before the analysis to obtain final glucose concentrations within the assay calibration range (this also reduced the concentrations of other matrix components, thus minimizing a possible matrix effect). In addition, as an example of a possible application of this device in the clinical field, we analysed glucose-spiked artificial serum samples (to comply with the calibration range of the ECL device, samples were preliminarily diluted 1:10 (v/v) with water). Table 1 shows the comparison between the glucose concentrations measured with the ECL device and the

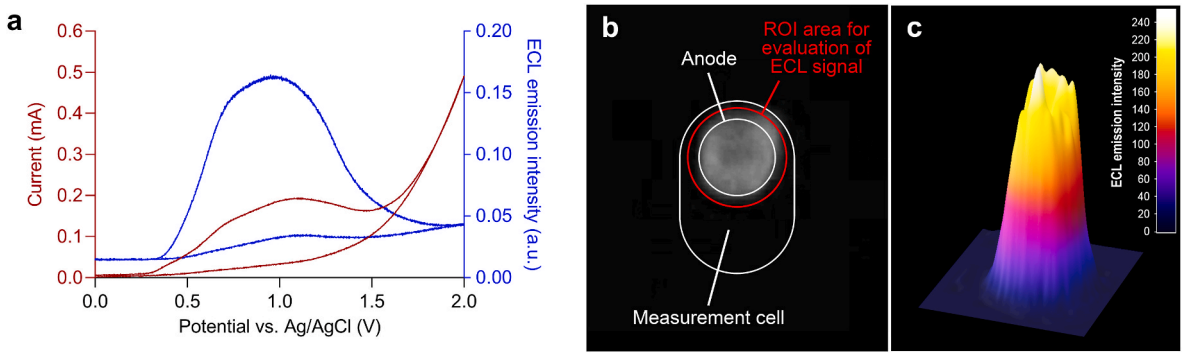

Fig. 2. (a) Profiles of current (red trace) and ECL emission intensity (blue trace) recorded in a CV/ECL experiment performed in the ECL device. (b) Image and (c) profile of the spatial distribution of the ECL emission (the real dimensions of the measurement cell and of the anode of the ECL device, as well the integration area used for the evaluation of the signal, are also shown). The measurements were carried out in carbonate buffer at pH 10.8 containing 5 mmol L^{-1} luminol and 0.1 mmol L^{-1} H_2O_2.

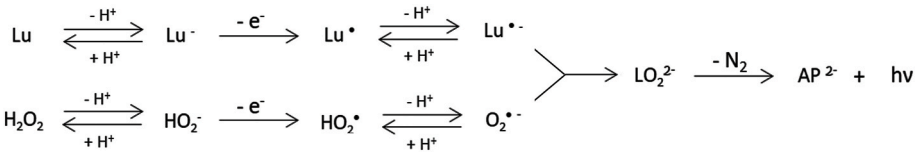

Scheme 1. Sequence of reactions leading to the generation of ECL emission by luminol and H_2O_2 in a carbonate buffer solution (pH 10.8) according to the mechanism proposed in Zhou et al. (2022). Lu: luminol, Lu^-: luminol anion, $Lu^{\bullet}$: luminol radical, $Lu^{\bullet-}$: luminol radical anion, H_2O_2: hydrogen peroxide, HO_2^-: hydrogen peroxide anion, $HO_2^{\bullet}$: hydrogen peroxide radical, $O_2^{\bullet-}$: superoxide radical anion, LO_2^{2-}: luminol peroxide compound, AP $^{2-}$: 3-aminophthalate dianion.

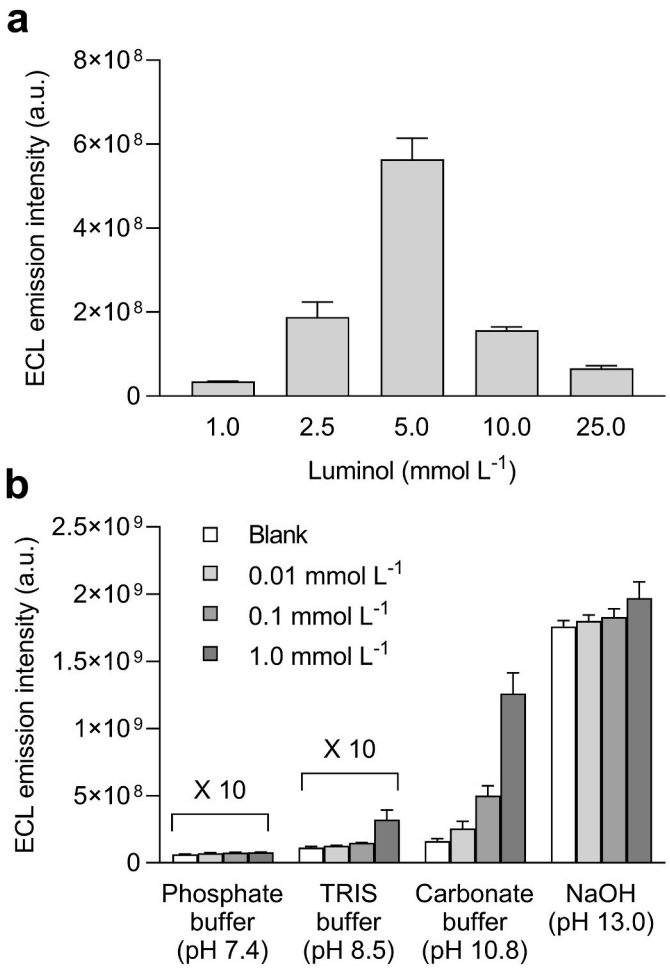

Fig. 3. (a) ECL maximum emission intensities obtained for a 0.1 mmol L^{-1} H_2O_2 solution in the presence of different luminol concentrations. The measurements were carried out in carbonate buffer at pH 10.8. (b) ECL maximum emission intensities obtained at different pH values in the presence of 5.0 mmol L^{-1} luminol and various concentrations of H_2O_2 (the ECL signals obtained in phosphate and TRIS buffers were plotted at ten times their real intensities). Each data is the mean ± SD of three independent measurements.

glucose contents, which have been also confirmed by using a reference enzymatic colorimetric assay. The recovery values varied between 86% and 112% and the assay reproducibility was satisfactory (CV% not higher than 10%), thus indicating the applicability of the ECL biosensor for the quantification of glucose in real matrices.

3.2. Hydrogel-based ECL device

To obtain an ECL glucose biosensor suitable for onsite application, we further simplified the analytical system by employing a 1.5 V AA alkaline battery to provide the voltage and using a smartphone for measuring the ECL emission. A 3D-printed dark box was designed to employ a Samsung S20 smartphone for the measurement (however, the dark box could be adapted with minimal modifications to other smartphones).

We also investigated the possibility to preload the reagents in the device within a hydrogel matrix, which will allow to prepare in advance the ECL devices and reduce the analytical procedure to the sample addition, incubation, and measurement steps. The prerequisites for the hydrogel matrix were inertness towards analytes, reagents, and electrode materials, as well as suitability as a reaction medium for the enzyme reaction and the ECL detection of hydrogen peroxide. Low-cost and environmental friendliness were also desirable characteristics. Based on these requirements, agarose was selected as the best candidate. Agarose gels are cheap, non-toxic, easy to prepare, they exhibit thermoreversible gelation, and are highly transparent in the visible range, thus allowing transmission and imaging of the optical signal (Calabria et al., 2021a, de Poulpiquet et al. N. 2016, Nguyen et al., 2020; Zarrintaj et al., 2018). Moreover, the agarose hydrogel acts as a protective carrier for the enzyme and enable easy diffusion of low molecular weight molecules such as glucose, H_2O_2, and luminol, thus ensuring a rapid response of the ECL biosensor.

3.2.1. Quantification of hydrogen peroxide

The hydrogel-based ECL device was preliminarily characterized to assess the effect of the hydrogel matrix on its performance. The CV/ECL experiments performed in the presence of H_2O_2 indicated that the maximum ECL emission intensity is obtained at a potential of about 0.75 V vs. Ag/AgCl, thus close to the value found for the solution ECL device (Fig. 5a). Notice that the maximum of ECL intensity for the hydrogel device is two times higher compared with conventional ECL device (see Fig. 2a) with almost the same current involved as evidence of higher performance of hydrogel-based sensor. Furthermore, the ECL emission kinetics was unaffected by the hydrogel matrix (Fig. 5b); since the peak ECL signal was reached a few seconds after voltage application, a 60-s ECL signal acquisition time was used also for smartphone-based experiments.

Then, the ECL device with luminol-loaded hydrogel was employed for analysing H_2O_2 standard solutions employing the 3D printed dark box and smartphone-based ECL detection. Fig. 6a shows the H_2O_2 calibration curve, which indicated an excellent linearity of response in the range 0.02–2.0 mmol L^{-1} of H_2O_2, as well as a LOD of 30 μmol L^{-1} of H_2O_2.

3.2.2. Quantification of glucose

Then, the ECL device with luminol/GO-loaded hydrogel was employed for glucose quantification. Fig. 6b and c show, respectively, the ECL images acquired by analysing glucose standard solutions with concentrations ranging from 0.05 to 5.0 mmol L^{-1} and the corresponding glucose calibration curve. By combining the end-point enzymatic method for glucose in the hydrogel matrix with the smartphone-based ECL detection of H_2O_2, a response proportional to the glucose concentration was obtained. The LOD of the assay (60 μmol L^{-1} of glucose) was almost the same found for the solution-based ECL device. It is worthwhile to note that in the hydrogel ECL device the GO-catalysed enzymatic reaction could be carried out at the alkaline pH required for the ECL measurement. Indeed, the coupling of the detection of H_2O_2 by

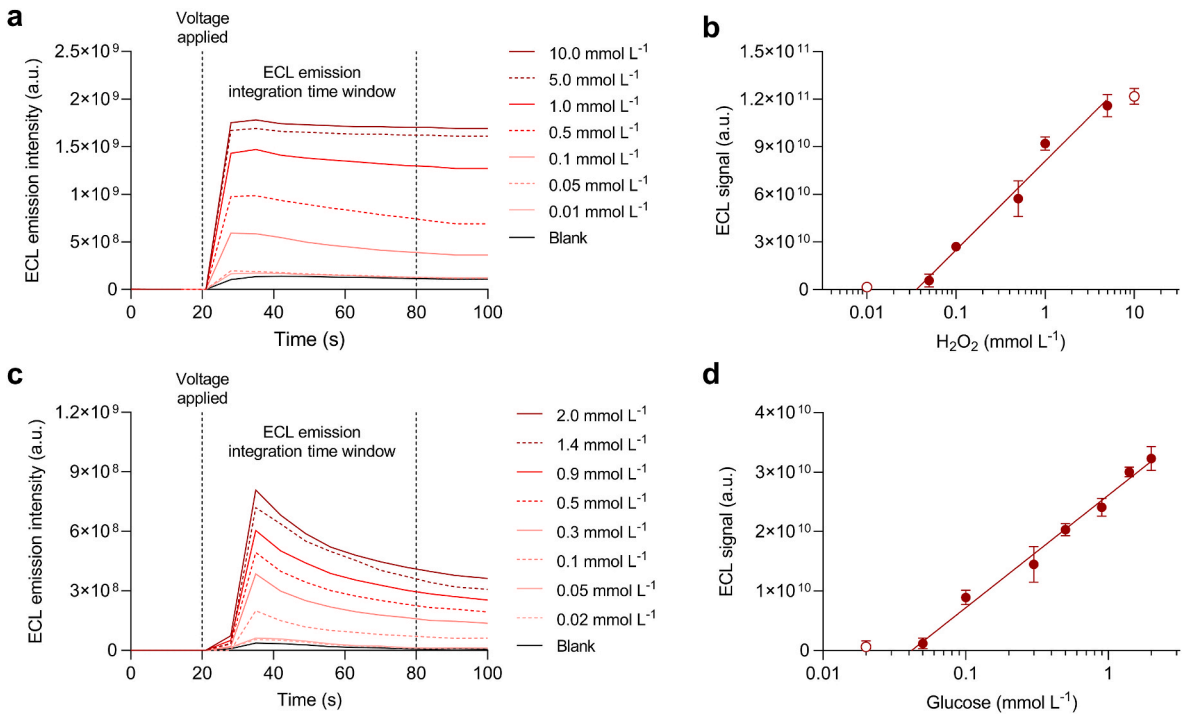

Fig. 4. (a) Kinetic profiles of the ECL emission obtained for the analysis of samples with different concentrations of H_2O_2 with the solution ECL device and (b) corresponding calibration curve for H_2O_2. The equation of the calibration curve in the 0.05 - 5.0 mmol L^{-1} concentration interval (filled circles) is $Y = (5.60 \pm 0.51) \times 10^{10} X + (8.09 \pm 0.41) \times 10^{10}$ ($R^2 = 0.97$), where Y and X are the ECL signal (after blank subtraction) and the logarithm of the concentration of H_2O_2 (mmol L^{-1}), respectively. (c) Kinetic profiles of the ECL emission obtained for the analysis of samples with different glucose concentrations with the solution ECL device and (d) corresponding calibration curve for glucose. The equation of the calibration curve in the 0.05 - 2.0 mmol L^{-1} concentration interval (filled circles) is $Y = (1.89 \pm 0.09) \times 10^{10} X + (2.61 \pm 0.06) \times 10^{10}$ ($R^2 = 0.99$), where Y and X are the ECL signal (after blank subtraction) and the logarithm of the concentration of glucose (mmol L^{-1}), respectively. Each data is the mean ± SD of three independent measurements.

Table 1
Results obtained by analyzing real samples.[a]

Glucose saline solutions[b]						
		Solution-based ECL device		Hydrogel-based ECL device		Reference assay
Sample no.	Nominal glucose concentration (% (m/v))	Measured glucose concentration (% (m/v))	Recovery (%)	Measured glucose concentration (% (m/v))	Recovery (%)	Measured glucose concentration (% (m/v))
#1	5.0	4.3 ± 0.1	86%	4.5 ± 0.4	90%	4.8 ± 0.1
#2	10.0	10.5 ± 0.7	105%	10.3 ± 0.7	103%	10.2 ± 0.4
#3	20.0	21.2 ± 0.6	106%	22.0 ± 1.1	110%	20.5 ± 0.6
#4	33.0	30.0 ± 1.3	91%	30.9 ± 2.6	94%	32.2 ± 0.5
#5	50.0	48.9 ± 1.9	98%	47.9 ± 2.9	96%	49.3 ± 0.9
#6	70.0	78.1 ± 4.4	112%	76.3 ± 5.8	109%	72.8 ± 1.7
Glucose-spiked artificial serum samples[c]						
		Solution-based ECL device		Hydrogel-based ECL device		Reference assay
Sample no.	Spiked glucose concentration (mmol L^{-1})	Measured glucose concentration (mmol L^{-1})	Recovery (%)	Measured glucose concentration (mmol L^{-1})	Recovery (%)	Measured glucose concentration (mmol L^{-1})
#1	1.0	1.1 ± 0.1	110%	1.1 ± 0.1	110%	0.9 ± 0.1
#2	5.0	5.4 ± 0.2	108%	5.2 ± 0.3	104%	5.1 ± 0.1
#3	10.0	10.2 ± 0.5	102%	10.3 ± 0.7	103%	10.1 ± 0.3

[a] Results are the mean ± SD of three independent measurements.
[b] Glucose saline solutions were diluted 1:2000 (v/v) with water before analysis.
[c] Spiked artificial serum samples were diluted 1:10 (v/v) with water before analysis.

luminol's ECL with enzyme-catalysed reactions is often complicated by the requirement of a physiological pH for optimal enzyme activity (Fang et al., 2017). In such cases the enzyme reaction is often performed at a first stage and then the products are applied at the electrochemical cell (de Poulpiquet et al., 2016). The observation of GO enzyme activity at pH 10.8 is in line with previously reported findings showing that enzymes trapped in hydrogels displayed higher activity and increased tolerance to temperature and pH variation if compared with the free enzyme (Meyer et al., 2022).

To evaluate applicability of the biosensor, the real samples reported in paragraph 3.1.3, i.e., glucose saline solutions and glucose-spiked artificial serum samples, were analysed. As shown in Table 1, there was a quite good correspondence between the measured glucose concentrations and the expected values (recoveries ranged from 90% to 110%), and the assay reproducibility was satisfactory (CV% not higher than 10%).

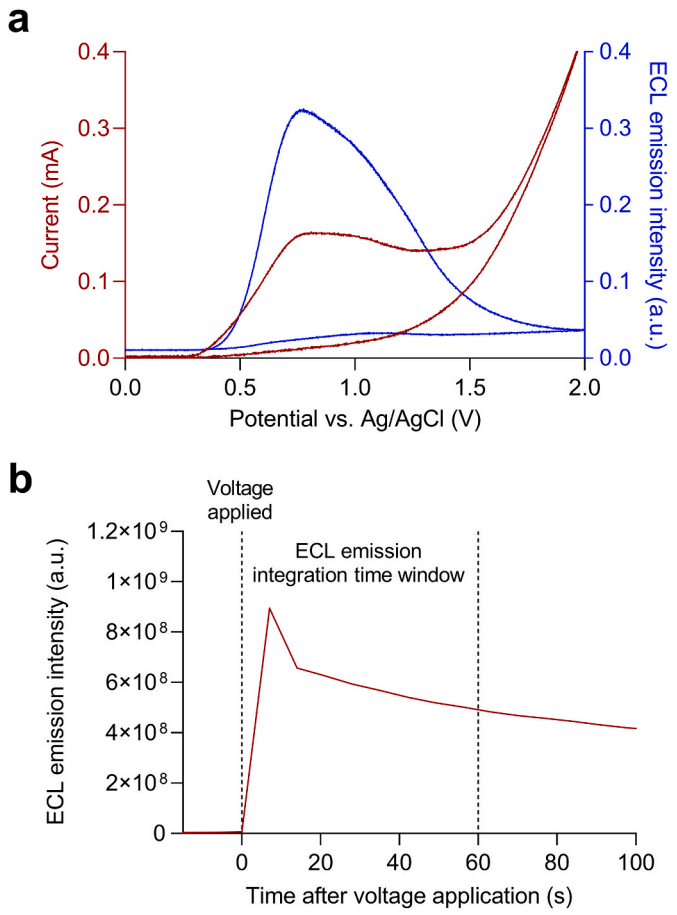

Fig. 5. (a) Profiles of current (red trace) and ECL emission intensity (blue trace) recorded in a CV/ECL experiment performed in the hydrogel ECL device and (b) kinetic profiles of the ECL emission. The measurements were carried out by employing a 0.1 mmol L^{-1} H_2O_2 standard solution.

The obtained results suggested the applicability of the hydrogel-based ECL device for assessing glucose blood levels. Furthermore, by considering that the expected blood glucose levels in healthy subjects are in the 3.9–7.1 mmol L^{-1} range (Danaei et al., 2011), both hypoglycaemic and hyperglycaemic samples could be discriminated.

The specificity of the ECL biosensor was evaluated by measuring the ECL signal corresponding to 0.2 mmol L^{-1} glucose in the presence of various interferents at the same concentration. Substances with reducing activity were tested, namely glycine, alanine, phenylalanine, dopamine, ascorbic acid, and uric acid. No interference was observed, as the biosensor response varied not more than 5% with respect to the glucose solution without interferents.

The stability of the hydrogel-based ECL device was evaluated by measuring the changes in the ECL signal obtained using devices stored in sealed plastic bags and in the dark at +4 °C for different times, up to four weeks. The response of biosensor was maintained for at least 3 weeks, showing the ability of the agarose gelled medium to preserve enzyme activity and reagents stability, as reported in Fig. 6d.

4. Conclusions

In this work an ECL-based enzymatic biosensor for glucose quantification was developed through a low-cost 3D printing technology and using a PLA sustainable polymer. The protocol for the detection of hydrogen peroxide based on the luminol/H_2O_2 ECL system was optimised and then applied for the quantification of H_2O_2 produced in the enzymatic oxidation of glucose catalysed by GO. The biosensor performance was initially evaluated using a CCD for ECL signal detection and a feasibility study was carried out for the quantification of glucose in pharmaceutical formulations. Since the use of a CCD camera reduced the portability of the biosensor and required expert personnel for the acquisition, processing and interpretation of the results, a further step towards the development of a real point-of-need analytical system was the implementation of a smartphone-based ECL signal measurement. In addition, the development of an ECL device containing a hydrogel matrix with preloaded reagents for a single-use disposable assay made it possible to considerably simplify the analytical protocol, which required only the addition of the sample (possibly preceded by its appropriate

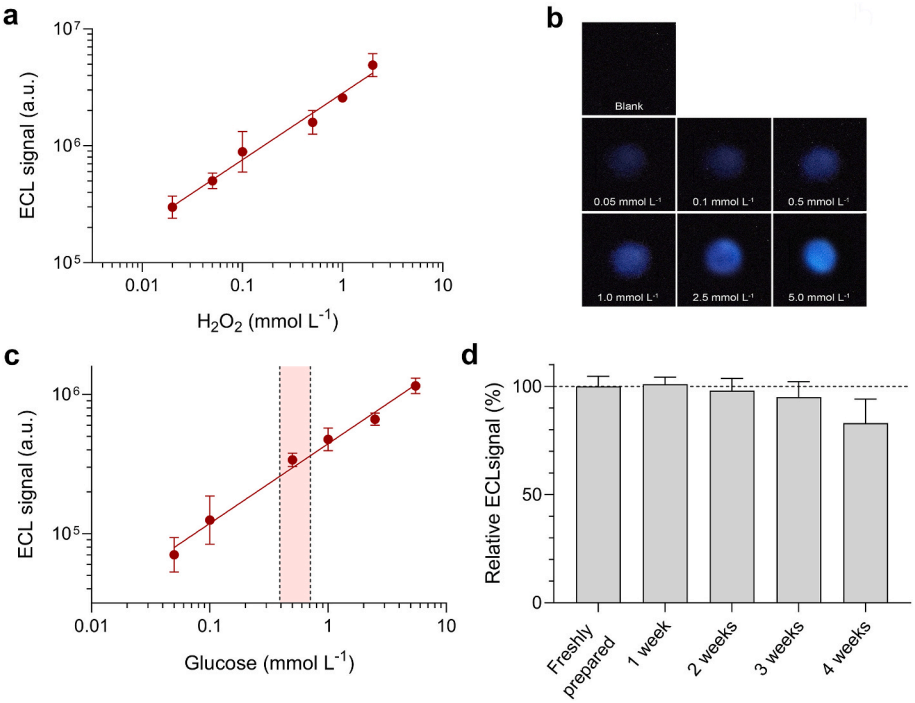

Fig. 6. (a) Calibration curve for the analysis of H_2O_2 obtained using the hydrogel-based ECL device. The equation of the calibration curve in the 0.02–2.0 mmol L^{-1} concentration interval is $Y = (0.57 \pm 0.04)$ $X + (6.45 \pm 0.04)$ ($R^2 = 0.98$), where Y and X are the logarithms of the ECL signal (after blank subtraction) and the concentration of H_2O_2 (mmol L^{-1}), respectively. (b) ECL images acquired with the smartphone during the analysis of glucose standard solutions. (c) Calibration curve for the analysis of glucose obtained using the hydrogel-based ECL device. The equation of the calibration curve in the 0.05–5.0 mmol L^{-1} concentration interval is $Y = (1.89 \pm 0.09) \times 10^{10}$ $X + (2.61 \pm 0.06) \times 10^{10}$ ($R^2 = 0.99$), where Y and X are the logarithms of the ECL signal (after blank subtraction) and the concentration of glucose (mmol L^{-1}), respectively. The shaded area indicates the expected range of blood glucose concentrations of healthy subjects upon 1:10 (v/v) dilution (as described in the text). (d) ECL signals obtained by analysing a 5 mmol L^{-1} glucose solution employing hydrogel-based ECL devices stored in sealed plastic bags and in the dark at +4 °C for different times. Each data is the mean ± SD of three independent measurements.

dilution). As an example of a possible point-of-care application of this analytical system, glucose-spiked artificial serum samples were analysed obtaining satisfactory results. With respect to previously reported ECL-based biosensors for glucose, the developed device enables easy and reproducible rapid prototyping of electrode components by 3D printing, as well as reagents preloading in a hydrogel matrix for convenient POC application. The developed device could therefore represent an advancement in the field of portable and low-cost ECL-based analytical systems and, although it has been used for glucose quantification, its application can in principle be extended to all those substrates that are converted into hydrogen peroxide by oxidases or for which there is a specific enzymatic reaction that can be coupled to a secondary reaction catalysed by an oxidase. In addition, the future combination of this platform with paper-based substrates would enhance its sustainable feature.

Declaration of competing interest

The authors declare the following financial interests/personal relationships which may be considered as potential competing interests: Massimo Guardigli and Francesco Paolucci report financial support was provided by MUR.

Data availability

Data will be made available on request.

Acknowledgements

This research was funded by the Italian Ministry of University and Research: PRIN2017 project “Cutting edge analytical chemistry methodologies and bio-tools to boost precision medicine in hormone-related diseases”, Prot. 2017Y2PAB8; and PRIN2017 project “Functional 3D architectures for electrochemiluminescence applications”, Prot. 2017FJCPEX.

References

Ali, M.A., Hu, C.S., Yttri, E.A., Panat, R., 2022. Recent advances in 3D printing of biomedical sensing devices. Adv. Funct. Mater. 32, 2107671 https://doi.org/10.1002/adfm.202107671.

Arshavsky-Graham, S., Enders, A., Ackerman, S., Bahnemann, J., Segal, E., 2021. 3D-printed microfluidics integrated with optical nanostructured porous aptasensors for protein detection. Microchim. Acta 188, 67. https://doi.org/10.1007/s00604-021-04725-0.

Aymard, C., Bonaventura, C., Henkens, R., Mousty, C., Hecquet, L., Charmantray, F., Blum, L.J., Doumeche, B., 2017. High-throughput electrochemical screening assay for free and immobilized oxidases: electrochemiluminescence and intermittent pulse amperometry. Chemelectrochem 4, 957–966. https://doi.org/10.1002/celc.201600647.

Basiaga, M., Paszenda, Z., Walke, W., Karasiński, P., Marciniak, J., 2014. Electrochemical impedance spectroscopy and corrosion resistance of SiO2 coated CpTi and Ti-6Al-7Nb alloy. In: Piętka, E., Kawa, J., Wieclawek, W. (Eds.), Information Technologies in Biomedicine, Volume 4, Advances in Intelligent Systems and Computing, vol. 284. Springer, Cham, pp. 411–420. https://doi.org/10.1007/978-3-319-06596-0_39.

Bhaiyya, M., Kulkarni, M.B., Pattnaik, P.K., Goel, S., 2022a. Internet of things-enabled photomultiplier tube- and smartphone-based electrochemiluminescence platform to detect choline and dopamine using 3D-printed closed bipolar electrodes. Luminescence 37, 357–365. https://doi.org/10.1002/bio.4179.

Bhaiyya, M., Pattnaik, P.K., Goel, S., 2022b. Multiplexed and simultaneous biosensing in a 3D-printed portable six-well smartphone operated electrochemiluminescence standalone point-of-care platform. Microchim. Acta 189, 79. https://doi.org/10.1007/s00604-022-05200-0.

Bishop, G.W., Satterwhite-Warden, J.E., Bist, I., Chen, E., Rusling, J.F., 2016. Electrochemiluminescence at bare and DNA-coated graphite electrodes in 3D-printed fluidic devices. ACS Sens. 1, 197–202. https://doi.org/10.1021/acssensors.5b00156.

Calabria, D., Guardigli, M., Severi, P., Trozzi, I., Pace, A., Cinti, S., Zangheri, M., Mirasoli, M., 2021a. A smartphone-based chemosensor to evaluate antioxidants in agri-food matrices by in situ AuNP formation. Sensors 21, 5432. https://doi.org/10.3390/s21165432.

Calabria, D., Mirasoli, M., Guardigli, M., Simoni, P., Zangheri, M., Severi, P., Caliceti, C., Roda, A., 2020. Paper-based smartphone chemosensor for reflectometric on-site total polyphenols quantification in olive oil. Sensor. Actuator. B Chem. 305, 127522 https://doi.org/10.1016/j.snb.2019.127522.

Calabria, D., Zangheri, M., Trozzi, I., Lazzarini, E., Pace, A., Mirasoli, M., Guardigli, M., 2021b. Smartphone-based chemiluminescent origami mu PAD for the rapid assessment of glucose blood levels. Biosensors 11, 381. https://doi.org/10.3390/bios11100381.

Cardoso, R.M., Kalinke, C., Rocha, R.G., dos Santos, P.L., Rocha, D.P., Oliveira, P.R., Janegitz, B.C., Bonacin, J.A., Richter, E.M., Munoz, R.A.A., 2020. Additive-manufactured (3D-printed) electrochemical sensors: a critical review. Anal. Chim. Acta 1118, 73–91. https://doi.org/10.1016/j.aca.2020.03.028.

Chiado, A., Palmara, G., Chiappone, A., Tanzanu, C., Pirri, C.F., Roppolo, I., Frascella, F., 2020. A modular 3D printed lab-on-a-chip for early cancer detection. Lab Chip 20, 665–674. https://doi.org/10.1039/c9lc01108k.

Climent, E., Rurack, K., 2021. Combining electrochemiluminescence detection with aptamer-gated indicator releasing mesoporous nanoparticles enables ppt sensitivity for strip-based rapid tests. Angew. Chem., Int. Ed. Engl. 60, 26287–26297. https://doi.org/10.1002/anie.202110744.

Danaei, G., Finucane, M.M., Lu, Y., Singh, G.M., Cowan, M.J., Paciorek, C.J., Lin, J.K., Farzadfar, F., Khang, Y.H., Stevens, G.A., Rao, M., Ali, M.K., Riley, L.M., Robinson, C. A., Ezzati, M., 2011. National, regional, and global trends in fasting plasma glucose and diabetes prevalence since 1980: systematic analysis of health examination surveys and epidemiological studies with 370 country-years and 2·7 million participants. Lancet 378, 31–40. https://doi.org/10.1016/S0140-6736(11)60679-X.

de Poulpiquet, A., Diez-Buitrago, B., Milutinovic, M.D., Sentic, M., Arbault, S., Bouffier, L., Kuhn, A., Sojic, N., 2016. Dual enzymatic detection by bulk electrogenerated chemiluminescence. Anal. Chem. 88, 6585–6592. https://doi.org/10.1021/acs.analchem.6b01434.

Delaney, J.L., Hogan, C.F., Tian, J., Shen, W., 2011. Electrogenerated chemiluminescence detection in paper-based microfluidic sensors. Anal. Chem. 83, 1300–1306. https://doi.org/10.1021/ac102392t.

Doeven, E.H., Barbante, G.J., Harsant, A.J., Donnelly, P.S., Connell, T.U., Hogan, C.F., Francis, P.S., 2015. Mobile phone-based electrochemiluminescence sensing exploiting the ’USB On-The-Go’ protocol. Sensor. Actuator. B Chem. 216, 608–613. https://doi.org/10.1016/j.snb.2015.04.087.

Douman, S.F., De Eguilaz, M.R., Cumba, L.R., Beirne, S., Wallace, G.G., Yue, Z.L., Iwuoha, E.I., Forster, R.J., 2021. Electrochemiluminescence at 3D printed titanium electrodes. Front. Chem. 9, 662810 https://doi.org/10.3389/fchem.2021.662810.

Du, F.X., Chen, Y.Q., Meng, C.D., Lou, B.H., Zhang, W., Xu, G.B., 2021. Recent advances in electrochemiluminescence immunoassay based on multiple-signal strategy. Curr. Opin. Electrochem. 28, 100725 https://doi.org/10.1016/j.coelec.2021.100725.

Fang, C., Li, H., Yan, J., Guo, H., Yifeng, T., 2017. Progress of the electrochemiluminescence biosensing strategy for clinical diagnosis with luminol as the sensing probe. Chemelectrochem 4, 1587–1593. https://doi.org/10.1002/celc.201700465.

Fiorani, A., Merino, J.P., Zanut, A., Criado, A., Valenti, G., Prato, M., Paolucci, F., 2019. Advanced carbon nanomaterials for electrochemiluminescent biosensor applications. Curr. Opin. Electrochem. 16, 66–74. https://doi.org/10.1016/j.coelec.2019.04.018.

Gao, C.M., Yu, H.H., Wang, Y.H., Liu, D.Z., Wen, T., Zhang, L.N., Ge, S.G., Yu, J.H., 2020. Paper-based constant potential electrochemiluminescence sensing platform with black phosphorus as a luminophore enabled by a perovskite solar cell. Anal. Chem. 92, 6822–6826. https://doi.org/10.1021/acs.analchem.0c01033.

Gao, W.Y., Muzyka, K., Ma, X.G., Lou, B.H., Xu, G.B., 2018. A single-electrode electrochemical system for multiplex electrochemiluminescence analysis based on a resistance induced potential difference. Chem. Sci. 9, 3911–3916. https://doi.org/10.1039/c8sc00410b.

Hesari, M., Ding, Z., 2015. Review—electrogenerated chemiluminescence: light years ahead. J. Electrochem. Soc. 163, H3116–H3131. https://doi.org/10.1149/2.0161604jes.

Huang, X.W., Xu, D.D., Chen, J., Liu, J.X., Li, Y.B., Song, J., Ma, X., Guo, J.H., 2018. Smartphone-based analytical biosensors. Analyst 143, 5339–5351. https://doi.org/10.1039/c8an01269e.

Kadimisetty, K., Malla, S., Rusling, J.F., 2017. Automated 3-D printed arrays to evaluate genotoxic chemistry: e-cigarettes and water samples. ACS Sens. 2, 670–678. https://doi.org/10.1021/acssensors.7b00118.

Kalkal, A., Kumar, S., Kumar, P., Pradhan, R., Willander, M., Packirisamy, G., Kumar, S., Malhotra, B.D., 2021. Recent advances in 3D printing technologies for wearable (bio)sensors. Addit. Manuf. 46, 102088 https://doi.org/10.1016/j.addma.2021.102088.

Kitte, S.A., Gao, W., Zholudov, Y.T., Qi, L., Nsabimana, A., Liu, Z., Xu, G., 2017. Stainless steel electrode for sensitive luminol electrochemiluminescent detection of H_2O_2, glucose, and glucose oxidase activity. Anal. Chem. 89, 9864–9869. https://doi.org/10.1021/acs.analchem.7b01939.

Lai, W.Q., Chang, Y.F., Chou, F.N., Yang, D.M., 2022. Portable FRET-based biosensor device for on-site lead detection. Biosensors 12, 157. https://doi.org/10.3390/bios12030157.

Leca-Bouvier, B., Doumèche, B., Blum, L.J., 2020. Enzymatic assays. In: Sojic, N. (Ed.), Analytical Electrogenerated Chemiluminescence: from Fundamentals to Bioassays. The Royal Society of Chemistry, London, pp. 331–385. https://doi.org/10.1039/9781788015776-00331.

Lertvachirapaiboon, C., Baba, A., Shinbo, K., Kato, K., 2021. Dual-mode surface plasmon resonance sensor chip using a grating 3D-printed prism. Anal. Chim. Acta 1147, 23–29. https://doi.org/10.1016/j.aca.2020.12.027.

Li, S., Liu, J.L., Chen, Z.T., Lu, Y.L., Low, S.S., Zhu, L.H., Cheng, C., He, Y., Chen, Q.M., Su, B., Liu, Q.J., 2019. Electrogenerated chemiluminescence on smartphone with

graphene quantum dots nanocomposites for Escherichia coli detection. Sensor. Actuator. B Chem. 297, 126811 https://doi.org/10.1016/j.snb.2019.126811.
Li, X.C., Yang, F., Wong, J.X.H., Yu, H.Z., 2017. Integrated smartphone-app-chip system for on-site parts-per-billion-level colorimetric quantitation of aflatoxins. Anal. Chem. 89, 8908–8916. https://doi.org/10.1021/acs.analchem.7b01379.
Liu, T., Wang, W.Q., Ding, H., Liu, Z.Q., Zhang, S.Z., Yi, D.R., 2020. Development of a handheld dual-channel optical fiber fluorescence sensor based on a smartphone. Appl. Opt. 59, 601–606. https://doi.org/10.1364/AO.378622.
Liu, Z., Qi, W., Xu, G., 2015. Recent advances in electrochemiluminescence. Chem. Soc. Rev. 44, 3117–3142. https://doi.org/10.1039/C5CS00086F.
Lv, W.X., Ye, H.C., Yuan, Z.Q., Liu, X.J., Chen, X., Yang, W.S., 2020. Recent advances in electrochemiluminescence-based simultaneous detection of multiple targets. Trac. Trends Anal. Chem. 123, 115767 https://doi.org/10.1016/j.trac.2019.115767.
Ma, X., Gao, W., Du, F., Yuan, F., Yu, J., Guan, Y., Sojic, N., Xu, G., 2021. Rational design of electrochemiluminescent devices. Acc. Chem. Res. 54, 2936–2945. https://doi.org/10.1021/acs.accounts.1c00230.
Marzo, A.M.L., Mayorga-Martinez, C.C., Pumera, M., 2020. 3D-printed graphene direct electron transfer enzyme biosensors. Biosens. Bioelectron. 151, 111980 https://doi.org/10.1016/j.bios.2019.111980.
Meyer, J., Meyer, L.-E., Kara, S., 2022. Enzyme immobilization in hydrogels: a perfect liaison for efficient and sustainable biocatalysis. Eng. Life Sci. 22, 165–177. https://doi.org/10.1002/elsc.202100087.
Miao, W., 2008. Electrogenerated chemiluminescence and its biorelated applications. Chem. Rev. 108, 2506–2553. https://doi.org/10.1021/cr068083a.
Motaghi, H., Ziyaee, S., Mehrgardi, M.A., Kajani, A.A., Bordbar, A.K., 2018. Electrochemiluminescence detection of human breast cancer cells using aptamer modified bipolar electrode mounted into 3D printed microchannel. Biosens. Bioelectron. 118, 217–223. https://doi.org/10.1016/j.bios.2018.07.066.
Mustafa, F., Carhart, M., Andreescu, S., 2021. A 3D-printed breath analyzer incorporating CeO2 nanoparticles for colorimetric enzyme-based ethanol sensing. ACS Appl. Nano Mater. 4, 9361–9369. https://doi.org/10.1021/acsanm.1c01826.
Nasrollahpour, H., Khalilzadeh, B., Naseri, A., Sillanpää, M., Chia, C.H., 2022. Homogeneous electrochemiluminescence in the sensors game: what have we learned from past experiments? Anal. Chem. 94, 349–365. https://doi.org/10.1021/acs.analchem.1c03909.
Nguyen, P.T., Ahn, H.T., Kim, M.I., 2020. Reagent-free colorimetric assay for galactose using agarose gel entrapping nanoceria and galactose oxidase. Nanomaterials 10, 895. https://doi.org/10.3390/nano10050895.
Nikolaou, P., Sciuto, E.L., Zanut, A., Petralia, S., Valenti, G., Paolucci, F., Prodi, L., Conoci, S., 2022. Ultrasensitive PCR-Free detection of whole virus genome by electrochemiluminescence. Biosens. Bioelectron. 209, 114165 https://doi.org/10.1016/j.bios.2022.114165.
Omar, M.H., Razak, K.A., Ab Wahab, M.N., Hamzah, H.H., 2021. Recent progress of conductive 3D-printed electrodes based upon polymers/carbon nanomaterials using a fused deposition modelling (FDM) method as emerging electrochemical sensing devices. RSC Adv. 11, 16557–16571. https://doi.org/10.1039/d1ra01987b.
Palenzuela, C.L.M., Pumera, M., 2018. (Bio)Analytical chemistry enabled by 3D printing: sensors and biosensors. Trac. Trends Anal. Chem. 103, 110–118. https://doi.org/10.1016/j.trac.2018.03.016.
Pan, J.B., Chen, Z.G., Yao, M.C., Li, X.C., Li, Y.B., Sun, D.P., Yu, Y.Y., 2014. A two-electrode system-based electrochemiluminescence detection for microfluidic capillary electrophoresis and its application in pharmaceutical analysis. Luminescence 29, 427–432. https://doi.org/10.1002/bio.2565.
Pittet, P., Lu, G.N., Galvan, J.M., Ferrigno, R., Blum, L.J., Leca-Bouvier, B., 2007. PCB-based integration of electrochemiluminescence detection for microfluidic systems. Analyst 132, 409–411. https://doi.org/10.1039/b701296a.
Pittet, P., Lu, G.N., Galvan, J.M., Ferrigno, R., Stephan, K., Blum, L.J., Leca-Bouvier, B., 2008. A novel low-cost approach of implementing electrochemiluminescence detection for microfluidic analytical systems. Mater. Sci. Eng. C 28, 891–895. https://doi.org/10.1016/j.msec.2007.10.030.
Qi, H., Zhang, C., 2020. Electrogenerated chemiluminescence biosensing. Anal. Chem. 92, 524–534. https://doi.org/10.1021/acs.analchem.9b03425.
Quesada-Gonzalez, D., Merkoci, A., 2017. Mobile phone-based biosensing: an emerging "diagnostic and communication" technology. Biosens. Bioelectron. 92, 549–562. https://doi.org/10.1016/j.bios.2016.10.062.
Rahmawati, I., Einaga, Y., Ivandini, T.A., Fiorani, A., 2022. Enzymatic biosensors with electrochemiluminescence transduction. Chemelectrochem 9, 202200175. https://doi.org/10.1002/celc.202200175.
Richter, M.M., 2004. Electrochemiluminescence (ECL). Chem. Rev. 104, 3003–3036. https://doi.org/10.1021/cr020373d.
Roda, A., Mirasoli, M., Dolci, L.S., Buragina, A., Bonvicini, F., Simoni, P., Guardigli, M., 2011. Portable device based on chemiluminescence lensless imaging for personalized diagnostics through multiplex bioanalysis. Anal. Chem. 83, 3178–3185. https://doi.org/10.1021/ac200360k.
Roda, A., Zangheri, M., Calabria, D., Mirasoli, M., Caliceti, C., Quintavalla, A., Lombardo, M., Trombini, C., Simoni, P., 2019. A simple smartphone-based thermochemiluminescent immunosensor for valproic acid detection using 1,2-dioxetane analogue-doped nanoparticles as a label. Sensor. Actuator. B Chem. 279, 327–333. https://doi.org/10.1016/j.snb.2018.10.012.
Silva, L.R.G., Stefano, J.S., Orzari, L.O., Brazaca, L.C., Carrilho, E., Marcolino, L.H., Bergamini, M.F., Munoz, R.A.A., Janegitz, B.C., 2022. Electrochemical biosensor for SARS-CoV-2 cDNA detection using AuPs-modified 3D-printed graphene electrodes. Biosensors 12, 622. https://doi.org/10.3390/bios12080622.
Sojic, N., 2020. Analytical electrogenerated chemiluminescence: from fundamentals to bioassays. In: Detection Science Series No, vol. 15. The Royal Society of Chemistry, London.
Tsuge, T., Natsuaki, O., Ohashi, K., 1975. Purification, properties, and molecular features of glucose oxidase from *Aspergillus niger*. J. Biochem. 78, 835–843. https://doi.org/10.1093/oxfordjournals.jbchem.a130974.
Van Nguyen, H., Lee, E.Y., Seo, T.S., 2019. Point-of-care genetic analysis for multiplex pathogenic bacteria on a fully integrated centrifugal microdevice with a large-volume sample. Biosens. Bioelectron. 136, 132–139. https://doi.org/10.1016/j.bios.2019.04.035.
Wang, S.W., Dai, W.J., Ge, L., Yan, M., Yu, J.H., Song, X.R., Ge, S.G., 2012. Rechargeable battery-triggered electrochemiluminescence detection on microfluidic origami immunodevice based on two electrodes. Chem. Commun. 48, 9971–9973. https://doi.org/10.1039/c2cc34649d.
Yao, Y., Li, H.J., Wang, D., Liu, C.L., Zhang, C.S., 2017. An electrochemiluminescence cloth-based biosensor with smartphone-based imaging for detection of lactate in saliva. Analyst 142, 3715–3724. https://doi.org/10.1039/C7AN01008G.
Yoo, S.M., Jeon, Y.M., Heo, S.Y., 2022. Electrochemiluminescence systems for the detection of biomarkers: strategical and technological advances. Biosensors 12, 738. https://doi.org/10.3390/bios12090738.
Zangheri, M., Mirasoli, M., Guardigli, M., Di Nardo, F., Anfossi, L., Baggiani, C., Simoni, P., Benassai, M., Roda, A., 2019. Chemiluminescence-based biosensor for monitoring astronauts' health status during space missions: results from the International Space Station. Biosens. Bioelectron. 129, 260–268. https://doi.org/10.1016/j.bios.2018.09.059.
Zarrintaj, P., Manouchehri, S., Ahmadi, Z., Saeb, M.R., Urbanska, A.M., Kaplan, D.L., Mozafari, M., 2018. Agarose-based biomaterials for tissue engineering. Carbohydr. Polym. 187, 66–84. https://doi.org/10.1016/j.carbpol.2018.01.060.
Zhan, T.T., Su, Y., Lai, W., Chen, Z.Y., Zhang, C.S., 2022. A dry chemistry-based ultrasensitive electrochemiluminescence immunosensor for sample-to-answer detection of Cardiac Troponin I. Biosens. Bioelectron. 214, 114494 https://doi.org/10.1016/j.bios.2022.114494.
Zhang, H.R., Wang, Y.Z., Zhao, W., Xu, J.J., Chen, H.Y., 2016. Visual color-switch electrochemiluminescence biosensing of cancer cell based on multichannel bipolar electrode chip. Anal. Chem. 88, 2884–2890. https://doi.org/10.1021/acs.analchem.5b04716.
Zhang, Y., Cui, Y.Y., Sun, M.M., Wang, T.K., Liu, T., Dai, X.X., Zou, P., Zhao, Y., Wang, X.X., Wang, Y.Y., 2022. Deep learning-assisted smartphone-based molecularly imprinted electrochemiluminescence detection sensing platform: portable device and visual monitoring furosemide. Biosens. Bioelectron. 209, 114262 https://doi.org/10.1016/j.bios.2022.114262.
Zhou, P., Hu, S., Guo, W., Su, B., 2022. Deciphering electrochemiluminescence generation from luminol and hydrogen peroxide by imaging light emitting layer. Fundam. Res. 2, 682–687. https://doi.org/10.1016/j.fmre.2021.11.018.